ACS EARTH AND SPACE CHEMISTRY

Article

Cite This: ACS Earth Space Chem. 2019, 3, 2437−2442

http://pubs.acs.org/journal/aesccq

Plutonium(IV) Sorption during Ferrihydrite Nanoparticle Formation

Kurt F. Smith,[†,▽] Katherine Morris,[†] Gareth T. W. Law,[‡,§] Ellen H. Winstanley,[†] Francis R. Livens,[†,‡] Joshua S. Weatherill,[†] Liam G. Abrahamsen-Mills,[∥] Nicholas D. Bryan,[∥] J. Frederick W. Mosselmans,[⊥] Giannantonio Cibin,[⊥] Stephen Parry,[⊥] Richard Blackham,[#] Kathleen A. Law,[‡] and Samuel Shaw*[,†]

[†]Research Centre for Radwaste Disposal and Williamson Research Centre for Molecular Environmental Science, School of Earth and Environmental Sciences, The University of Manchester, Manchester, M13 9PL, United Kingdom

[‡]Centre for Radiochemistry Research, School of Chemistry, The University of Manchester, Manchester, M13 9PL, United Kingdom

[§]Radiochemistry Unit, Department of Chemistry, The University of Helsinki, A.I. Virtasen Aukio 1 (PL 55), 00014 Helsinki, Finland

[∥]National Nuclear Laboratory, Chadwick House, Warrington, WA3 6AE, United Kingdom

[⊥]Diamond Light Source Ltd, Diamond House, Harwell Science and Innovation Campus, Didcot, Oxfordshire OX11 0DE, United Kingdom

[#]Sellafield Ltd., Seascale, Cumbria CA20 1PG, United Kingdom

Supporting Information

ABSTRACT: Understanding interactions between iron (oxyhydr)oxide nanoparticles and plutonium is essential to underpin technology to treat radioactive effluents, in cleanup of land contaminated with radionuclides, and to ensure the safe disposal of radioactive wastes. These interactions include a range of adsorption, precipitation, and incorporation processes. Here, we explore the mechanisms of plutonium sequestration during ferrihydrite precipitation from an acidic solution. The initial 1 M HNO_3 solution with $Fe(III)_{(aq)}$ and $^{242}Pu(IV)_{(aq)}$ underwent controlled hydrolysis via the addition of NaOH to pH 9. The majority of $Fe(III)_{(aq)}$ and $Pu(IV)_{(aq)}$ was removed from solution between pH 2 and 3 during ferrihydrite formation. Analysis of Pu−ferrihydrite by extended X-ray absorption fine structure (EXAFS) spectroscopy showed that Pu(IV) formed an inner-sphere tetradentate complex on the ferrihydrite surface, with minor amounts of PuO_2 present. Best fits to the EXAFS data collected from Pu−ferrihydrite samples aged for 2 and 6 months showed no statistically significant change in the Pu(IV)−Fe oxyhydroxide surface complex despite the ferrihydrite undergoing extensive recrystallization to hematite. This suggests the Pu remains strongly sorbed to the iron (oxyhydr)oxide surface and could be retained over extended time periods.

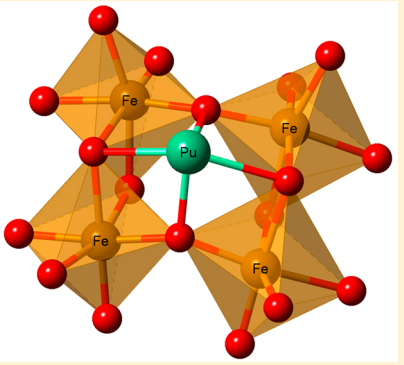

KEYWORDS: *Plutonium, ferrihydrite, hematite, nanoparticle, XAS, sorption*

INTRODUCTION

Plutonium is highly radiotoxic, long-lived (e.g., ^{239}Pu $t_{1/2}$ = 24,100 years) and ubiquitous in spent nuclear fuel and many radioactive wastes. It is a key risk driving radionuclide in contaminated land,[1] legacy nuclear facilities such as the Hanford Tanks and Sellafield Ponds,[2,3] and the treatment of radioactive effluents.[4] A key control on plutonium environmental mobility is via sorption reactions (i.e., surface adsorption and/or incorporation) with common mineral phases including iron (oxyhydr)oxides, e.g., ferrihydrite. Characterizing the atomic scale interactions of plutonium with mineral nanoparticles as they form is key to assessing its fate within contaminated environmental and radioactive waste geological disposal systems and in the development of effluent treatment technologies.

Ferrihydrite is the first Fe(III) hydrolysis product that forms from aqueous solution and is ubiquitous in environmental systems including natural waters, soils/sediments and living organisms.[5] Ferrihydrite nanoparticles (1−7 nm) have a large surface area (>200 m^2/g)[6] and high capacity to adsorb dissolved actinide aqueous species, including those of U, Np, and Pu.[7−9] Ferrihydrite forms via the hydrolysis of aqueous Fe(III) which proceeds via a multistep pathway where various polymeric ions form and coalesce to create nanoparticles.[10] Recently, it has been shown that the α-Fe_{13} Keggin ion can be a precursor to ferrihydrite formation when formed from an acid solution and that there is structural continuity from the Fe_{13} moiety to ferrihydrite.[10−12] The sorption properties of ferrihydrite are exploited in nuclear abatement technologies which sequester radionuclides from radioactive effluent streams. For example, the Enhanced Actinide Removal Plant (EARP; Sellafield Ltd.; U.K.) uses ferrihydrite precipitation to remove actinides including highly radiotoxic Pu and Am

Received: April 23, 2019
Revised: September 13, 2019
Accepted: September 16, 2019
Published: September 16, 2019

DOI: 10.1021/acsearthspacechem.9b00105
ACS Earth Space Chem. 2019, 3, 2437−2442

isotopes from acidic effluents.[4,13] In addition, precipitation of Fe(III) to decontaminate radioactive effluents has been explored in the context of the Fukushima Daiichi nuclear site in Japan.[14]

Several studies have characterized adsorption and redox processes occurring during the interaction of Pu with iron (oxyhydr)oxide surfaces.[9,15−23] The adsorption of Pu(V) to hematite (Fe_2O_3) and goethite (α-FeOOH) initiates a surface mediated reduction to Pu(IV), which can lead to the formation of $PuO_{2+x}\cdot nH_2O$ ($[Pu]_{tot} \geq 10^{-9}$ M).[20] The mechanism(s) controlling Pu(V) reduction have not been resolved with a range of processes proposed including electron shuttling, disproportionation, Pu(IV) stabilization at the surface, and Nernstian favorability of Pu(IV) complexes and colloids.[17] The adsorption of Pu(V) to magnetite (Fe_3O_4) leads to a surface mediated reduction to Pu(III). Here, X-ray absorption spectroscopy (XAS) in combination with Monte Carlo modeling indicates Pu(III) binds via three oxygens to three edge-sharing FeO_6 octahedra.[18] Other work has studied Pu(VI) interactions with goethite and showed the initial formation of an inner-sphere Pu(VI) adsorption complex which then underwent reduction to Pu(IV).[19] These Pu(IV) species are comparable to mononuclear U(IV) complexes which have been shown to form on iron (oxyhydr)oxide surfaces,[24−26] e.g., magnetite, upon reduction from U(VI). Overall, past work has indicated that Pu can adsorb to iron (oxyhydr)oxide surfaces via a variety of inner-sphere complexes and/or form discrete PuO_2 particles.[9,15−23] Despite this, there is currently no detailed information on the mechanism of Pu(IV) partitioning to solids during ferrihydrite formation. This information is crucial to determine key mechanisms of Pu uptake and retention during the radioactive effluent treatment process and, more broadly, within contaminated environments where both Pu and iron (oxyhydr)oxide phases are present.

Here, we characterize the mechanism of Pu(IV) uptake during ferrihydrite formation from an acidic solution containing Fe(III) and Pu(IV).[4,12] We gained a detailed insight into the speciation and molecular scale mechanisms of Pu(IV) sorption during nanoparticulate ferrihydrite formation and aging using a combination of aqueous chemical analyses, thermodynamic speciation modeling, and extended X-ray absorption fine structure (EXAFS) spectroscopy. Best fits to the EXAFS data show that Pu(IV) formed an inner-sphere tetradentate complex with the ferrihydrite and there was no statistically significant change in the Pu(IV) surface complex during sample aging despite clear evidence for crystallization of ferrihydrite to hematite and goethite. This provides important insights into the pathway of Pu uptake by ferrihydrite with implications for effluent treatment and understanding of Pu fate in engineered and natural environments.

METHODOLOGY

^{242}Pu is a highly radiotoxic, α-emitting radioisotope, and its possession and use is subject to strict statutory controls. A previously conditioned, 8 M HNO_3 and 0.03 M ^{242}Pu(IV) stock solution was used in these experiments, and UV−visible spectrophotometric (Shimadzu UV-2600) measurements taken on the stock immediately prior to the experiment confirmed the dominant oxidation state was Pu(IV) (see Figure S1).[27]

The Pu(IV) was spiked into a 1 M HNO_3, 7.2 mM Fe(III), solution to a final concentration of 2.0 μM ^{242}Pu(IV) (75 Bq mL^{-1}) and equilibrated overnight. This acidic solution is representative of typical EARP effluents treated at the Sellafield nuclear facility.[4,12] To initiate Fe(III) precipitation, an automated reaction vessel was used to control the pH during the addition of NaOH.[12] Initially, 7 M NaOH was introduced at a rate of 1.5 mL min^{-1} until pH 2.3, and then, the addition rate was reduced to 0.3 mL min^{-1} until pH 3. Finally, 0.2 M NaOH was added at a rate of 1.5 mL min^{-1} to pH 9 with the total reaction taking approximately 45 min. A control experiment without Pu was also undertaken to allow characterization of parallel, non-radioactive iron (oxyhydr)-oxide samples.

At selected points during the neutralization reaction, samples were removed and filtered (polyethersulfone, <0.22 μm). ^{242}Pu concentrations in solution were determined using α/β discriminated liquid scintillation (Quantulus). Dissolved Fe(III) concentrations were determined using hydroxylamine as a reductive agent coupled with the ferrozine assay method.[28,29] After 1 h at pH 9, a Pu−ferrihydrite suspension sample was removed and centrifuged (5000g; 5 min) to isolate the Pu doped ferrihydrite solid. The remaining Pu−ferrihydrite suspension was stored at 40 °C, and further solid samples were collected at 2 and 6 months of aging. A pH check on these aged samples confirmed the pH was maintained at 9 during aging. The fresh solid product and 2-month-aged sample from the non-radioactive control experiment were analyzed via X-ray diffraction (XRD,BrukerD8 Advance). An oxalate extraction method was used to quantify any recrystallization of Pu−ferrihydrite at the 6-month time point.[5] Here, 1 mL of Pu−ferrihydrite suspension was added to 1 mL of 0.02 M ammonium oxalate and 0.02 M oxalic acid at pH 3. The sample was then reacted in the absence of light for 2 h to dissolve any noncrystalline component (i.e., ferrihydrite).

Pu L_{III}-edge XAS spectroscopy analyses were conducted on B18 at Diamond Light Source at room temperature in fluorescence mode using a 32-element Ge detector and a bespoke transuranic sample holder for X-ray absorption spectroscopy to allow triple containment (Figure S2). All XANES data were calibrated against an in-line zirconium foil. Background processing was performed using Athena, and EXAFS modeling was carried out using Artemis (Demeter; 0.9.19)[30] and FEFF8.5L with self-consistency enabled.[31] XAS data were collected from solids (~1000 μg of ^{242}Pu g^{-1}) separated 1 h after the experiment was complete, and after aging the Pu−ferrihydrite suspension at pH 9 and 40 °C for 2 and 6 months. All speciation and saturation thermodynamic calculations were performed using PHREEQC (3.3.7)[32] coupled with R, a statistical programming language,[33,34] using the ANDRA SIT database (ThermoChimie v. 9a 2014).

RESULTS AND DISCUSSION

Analysis of the supernatant from the inactive control experiment indicated that Fe(III) was rapidly removed from solution between pH 1.5 and 3 (Figure 1). The behavior of Fe(III) was controlled via the precipitation of ferrihydrite and was consistent with thermodynamic predictions (Figure 1) and the results of previous studies.[4,12] The solid phase end product was two-line ferrihydrite, again consistent with past work[4,12] (Figure S3). XRD of the 2-month non-radioactive aging experiments confirmed significant recrystallization of ferrihydrite to dominantly hematite with minor goethite present (Figure S3). Oxalate extraction on the aged, Pu doped sample

DOI: 10.1021/acsearthspacechem.9b00105
ACS Earth Space Chem. 2019, 3, 2437−2442

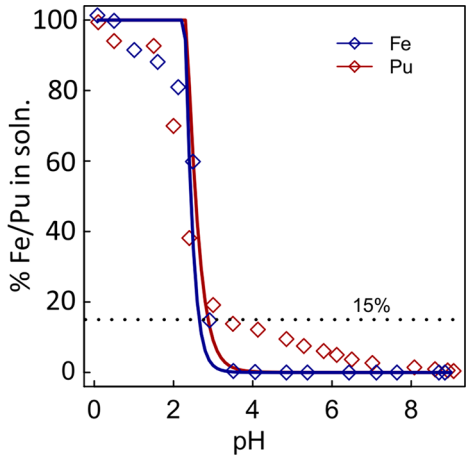

Figure 1. Normalized Pu (red) and Fe (blue) concentrations in supernatant. Red and blue lines represent model predictions assuming precipitation of $PuO_2{\cdot}2H_2O_{(am)}$ and ferrihydrite, respectively.

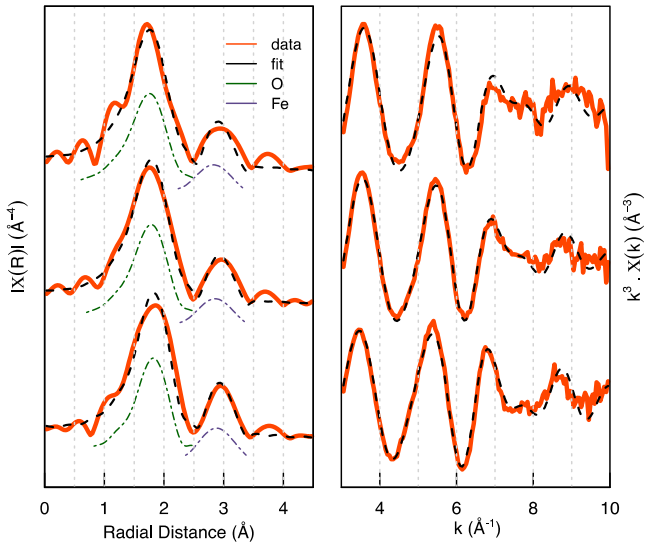

Figure 2. Right: Background subtracted Pu L_{III}-edge EXAFS spectra for fresh (bottom), 2-month (middle), and 6-month (top) samples. Left: Corresponding EXAFS Fourier transforms.

at 6 months confirmed >95% recrystallization to more ordered forms (e.g., hematite).

During base addition, the solution Pu concentration as a function of pH (Figure 1) showed approximately 85% of Pu was removed from solution contemporaneous with Fe(III) removal between pH 1.5 and 3. The remaining Pu (approximately 15%) was removed from solution as the base addition progressed to pH 9 (<0.2 Bq mL^{-1} detection limit). Interestingly, PHREEQC modeling of Pu(IV) concentration as a function of pH, which assumed that $PuO_2{\cdot}2H_2O_{(am)}$ precipitation controlled Pu(IV) concentration, reproduced a result broadly consistent with the experimental data except for the relatively slow removal of ∼15% of the Pu between pH 3 and 9 (Figure 1). However, the XAS data show that precipitation was not the dominant Pu(IV) sequestration mechanism (see below) and illustrates the essential value of experimental data underpinning thermodynamic modeling when inferring sorption processes.

The Pu XANES spectra from all samples were compared to published standards for Pu(III, IV, V, and VI) (Figure S4).[35] The edge position and structure of the XANES for all samples were essentially identical and closely matched the Pu(IV) standard, confirming that Pu was dominated by the +IV oxidation state in all of the samples. The background subtracted EXAFS spectra and corresponding Fourier transforms are shown in Figure 2. The EXAFS spectrum of the Pu associated with the freshly precipitated ferrihydrite was successfully modeled with an oxygen shell with eight scatterers at 2.34(1) Å. The substantial peak in the Fourier transform at 2.8 Å was attributed to Fe backscatterers and could best be modeled with four Fe atoms at 3.38(2) Å. The Debye−Waller factors are elevated (i.e., 0.014 and 0.015 $Å^2$, respectively) above those which would be normally expected for shells at these distances, typically ≤0.01 $Å^2$. This may indicate the O and Fe atoms surrounding the Pu are disordered and/or distributed over a range of distances. Additional fits with both O and Fe shells split yielded improved fits to the data and support the interpretation that both the O and Fe atoms are present at a range of distances, i.e., O = 2.22−2.40 Å and Fe = 3.28−3.45 Å (Table S1; Figure S5). However, the k range (3.0−10 $Å^{-1}$) of the EXAFS data suggests that the interatomic distance resolution will be approximately ±0.22 Å;[36] therefore, the data do not allow full resolution of interatomic distances in these samples. Regardless, within the resolution available, the data are entirely consistent with the formation of a Pu(IV) inner-sphere adsorption complex on the ferrihydrite surface. The EXAFS data from the 2- and 6-month-aged samples (Figure 2) were fitted with an essentially identical Pu local coordination environment, indicating that the Pu(IV) remains as a surface complex that was statistically indistinguishable from that associated with the freshly precipitated ferrihydrite (Table 1). Finally, there was an additional feature in the Fourier transform present in all samples at approximately 3.8 Å (Figure 2). It was possible to fit this peak with Pu scatterers at interatomic distances of ∼3.8 Å (Table S2, Figure S6). This interatomic distance is consistent with the Pu−Pu distance in PuO_2 (3.82 Å)[37] and suggests a small fraction of Pu in the sample may be present as PuO_2. The Pu−Pu coordination number increases (0.6 to 0.9) from the fresh to the 6-month-aged sample and suggests that PuO_2 accounts for approximately 5−8% of the Pu present in the samples assuming bulk PuO_2 formation (where 12 Pu atoms would be expected). The change in the Pu−Pu coordination numbers appears to cause the subtle changes in the EXAFS as a function of sample aging in the k = 7−10 $Å^{-1}$ region. This is consistent with previous studies which have noted the formation of PuO_2 on the surface of hematite.[21] However, it is clear that, even when considering the possibility of PuO_2 in the samples, the predominant species is a Pu(IV) inner-sphere tetradentate tetranuclear adsorption complex at all time points and that the rate of PuO_2 formation is slow.

PLUTONIUM SORPTION DURING FERRIHYDRITE FORMATION AND CRYSTALLIZATION

The presence of multiple iron scatterers in the fits to the EXAFS data clearly shows that Pu(IV) was directly associated with the iron (oxyhydr)oxide nanoparticles. This is interesting, as tetravalent actinide species are generally considered to undergo rapid hydrolysis to form AnO_2 solid phases,[38,39] and the dissolved Pu concentration with pH matches with thermodynamic predictions assuming $PuO_2{\cdot}2H_2O_{(am)}$ formation (Figure 1). However, the EXAFS fits do not support PuO_2 precipitation, as the overriding mechanism controlling Pu(IV)

DOI: 10.1021/acsearthspacechem.9b00105
ACS Earth Space Chem. 2019, 3, 2437−2442

Table 1. EXAFS Fitting Statistics from Pu−Iron (Oxyhydr)oxide Samples (Single Shell Fits)

sample	path	N^a	R (Å)	σ^2 (Å^2)	ΔE_0	$S0_2{}^a$	R-factor
fresh	Pu−O	8	2.34 ± 0.01	0.014 ± 0.001	5.64	1	0.014
	Pu−Fe	4	3.38 ± 0.02	0.015 ± 0.002			
2 months	Pu−O	8	2.31 ± 0.01	0.016 ± 0.001	5.67	1	0.013
	Pu−Fe	4	3.36 ± 0.02	0.017 ± 0.002			
6 months	Pu−O	8	2.29 ± 0.02	0.018 ± 0.001	5.31	1	0.016
	Pu−Fe	4	3.34 ± 0.02	0.018 ± 0.003			

[a]Fixed parameters. N represents the coordination number; R denotes the interatomic distance; σ^2 represents the Debye−Waller factor; ΔE_0 represents the energy shift from the calculated energy Fermi level; $S0_2$ denotes the amplitude reduction factor.

behavior in these systems as Pu(IV) in a PuO_2 environment would be coordinated by a single shell of 8 O atoms at ∼2.36 Å and 12 Pu at 3.82 Å.[36,37] This incompatibility with the PuO_2 structure and the clear identification of multiple Fe scatterers in the EXAFS data confirm that the large majority of Pu forms an inner-sphere complex with the ferrihydrite nanoparticles following coprecipitation and during crystallization to hematite.

Combining the information from the EXAFS fits with the ferrihydrite structure and formation mechanism, a model for the Pu(IV) sorption process can be constructed. The structure of ferrihydrite is based on the Fe_{13} Keggin moiety.[11] Furthermore, other work[12] showed that, in non-radioactive ferrihydrite formation experiments parallel to those in the current study, Keggin clusters form in solution below pH 1 and then aggregate with low molecular weight species (e.g., monomers) above pH 2 to form ferrihydrite nanoparticles. In the current experiment, the removal of Pu(IV) from solution was concomitant with both Fe removal from solution and ferrihydrite nanoparticle formation (Figure 1). In addition, approximately 15% of the Pu adsorbs following ferrihydrite precipitation after pH 3 and up to pH 9. Overall, the EXAFS data indicate that the Pu(IV) is sequestered via adsorption to the ferrihydrite nanoparticles. The variation in Pu−O distances observed for the adsorption complex (i.e., Pu−O distance from 2.22 to 2.4 Å, Table S1) is consistent with previous studies of Pu and other +IV actinide species, e.g., Th(IV), adsorption to iron (oxyhydr)oxides.[19,40] The shorter An−O distances are attributed to binding via surface oxygens and the longer distances as coordinating water molecules. The exact nature of the Pu(IV) tetranuclear complex on the ferrihydrite/hematite surface is unclear without additional information. However, one possibility is binding to the "square" window of the Fe_{13} Keggin unit, which is the key structural unit of ferrihydrite.[11] A recent study showed that Bi(III) can bind to the Keggin unit via this mechanism by attachment to four Fe−O octahedra, with Bi−Fe distances of ∼3.3−3.4 Å. The crystal radii of Bi(III) and Pu(IV) in 8-fold coordination are comparable (1.31 Å vs 1.10 Å).[41] Furthermore, the overall local environment of Bi(III) associated with this surface adsorption process is consistent with that of Pu(IV) associated with the freshly precipitated ferrihydrite, as determined by EXAFS analysis, i.e., four Pu−Fe 3.28−3.36 Å. The similarity in the local coordination environment raises the possibility that Pu(IV) is interacting with the surface of the ferrihydrite via a similar mechanism (see the Abstract graphic). However, it should be noted that the fits to the EXAFS data indicate that the Pu(IV) local environment does not change during ferrihydrite crystallization to hematite (Table 1), which does not contain the Fe_{13} Keggin structural unit. Clearly, Pu(IV) remains bound as an inner-sphere complex throughout extensive recrystallization of the ferrihydrite to more ordered forms (i.e., hematite). However, despite the new insights from the current work, the exact relationship of the Pu(IV) absorption complex to the surface structures of ferrihydrite and hematite is not fully resolved. In particular, it remains unclear whether the Pu(IV) is associated with the surface of the hematite or whether it becomes occluded in the hematite particle structure. Regardless, the Pu(IV) local environment derived from the EXAFS shows that Pu(IV) is stable as an inner-sphere complex in this dynamic system.

This proposed Pu(IV) tetradenate adsorption complex is consistent with similar Pu−Fe surface species reported in past work. For example, Hu et al.[19] observe Pu(IV) as an inner-sphere complex occupying a site on goethite with multiple Fe backscatterers (∼5) identified at ∼3.3 Å. Similarly, Kirsch et al.[18] observed that, upon reaction with magnetite, Pu(III) was linked via three oxygen atoms to three edge-sharing FeO_6 octahedra on the surface but with larger Pu−Fe distances (3.54 Å). The Pu(IV) adsorption complex is also comparable to U(IV) mononuclear complexes which form on the magnetite surface.[26] However, studies suggest the U(IV) forms a binuclear complex on magnetite at defect or lattice step/kink sites,[26] which is distinct from the tetradentate Pu(IV) adsorption species observed in this study. A recent study[42] also observed partial incorporation of Pu as Pu(III) following coprecipitation with magnetite. Here the Pu had a split Pu−O shell with four O scatterers at 2.22 and 2.45 Å attributed to a pyrochlore-like coordination environment within the structure. Overall, these results highlight that, for a range of environmentally relevant iron (oxyhydr)oxides, Pu(III, IV) adsorbs directly to the mineral surface and/or becomes incorporated.

IMPLICATIONS

Overall, the combined solution and EXAFS data presented show that Pu(IV) strongly adsorbs via an inner-sphere complex during ferrihydrite formation. The best EXAFS fit modeled for the Pu(IV) complex shows Pu(IV) is associated with the iron (oxyhydr)oxide surface via a tetradentate complex. This confirms that the previously predicted PuO_2 solid phase does not dominate in this system and indicates that during treatment of acidic radioactive effluents Pu(IV) will sorb extensively during the formation of ferrihydrite particles. This shows the highly effective nature of this treatment protocol for decontaminating Pu containing effluents. In addition, the Pu(IV)−Fe surface complex remains essentially unchanged during aging and crystallization to hematite, which highlights that Pu speciation is likely to remain stable during waste encapsulation and storage. Finally, the clear identification of a persistent and stable inner-sphere Pu(IV) adsorption complex lends weight to the growing body of literature identifying Pu(IV) adsorption complexes to iron (oxyhydr)oxides as

DOI: 10.1021/acsearthspacechem.9b00105
ACS Earth Space Chem. 2019, 3, 2437−2442

stable Pu species across a range of engineered and natural environments.

■ ASSOCIATED CONTENT

Supporting Information

The Supporting Information is available free of charge on the ACS Publications website at DOI: 10.1021/acsearthspacechem.9b00105.

UV spectra for the Pu stock solution and Pu(III, IV, V, VI) standards (Figure S1); photograph of the triple containment sample holder used for Pu XAS analysis (Figure S2); pXRD pattern for the fresh ferrihydrite precipitate and after 6 months of aging (Figure S3); XANES spectra for Pu−iron (oxyhydr)oxide solid and reference standards (Figure S4); EXAFS data tables (Tables S1 and S2), and figures (Figure S5 and S6) for alternative fits to the data (PDF)

■ AUTHOR INFORMATION

Corresponding Author

*E-mail: sam.shaw@manchester.ac.uk.

ORCID

Katherine Morris: 0000-0002-0716-7589
Gareth T. W. Law: 0000-0002-2320-6330
Joshua S. Weatherill: 0000-0002-8309-4473
J. Frederick W. Mosselmans: 0000-0001-6473-2743
Samuel Shaw: 0000-0002-6353-5454

Present Address

[∇]K.F.S.: Chemical Sciences Division, Lawrence Berkeley National Laboratory, Berkeley, CA 94720.

Notes

The authors declare no competing financial interest.

■ ACKNOWLEDGMENTS

This work was supported by Env Rad Net (ST/K001787/1 and ST/N002474/1) and by The University of Manchester, Sellafield Ltd., and the National Nuclear Laboratory via the Effluents Centre of Excellence. We thank Simon Kellet from Sellafield Ltd. for his support. We acknowledge Diamond Light Source for access to B18 provided by beamtime award SP17243.

■ REFERENCES

(1) Kersting, A.; Efurd, D.; Finnegan, D.; Rokop, D.; Smith, D.; Thompson, L. Migration of plutonium in ground water at the Nevada Test Site. *Nature* **1999**, *397*, 56−59.

(2) Peterson, R.; Buck, E.; Chun, J.; Daniel, R.; Herting, D.; Ilton, E.; Lumetta, G.; Clark, S. Review of the scientific understanding of radioactive waste at DOE Hanford site. *Environ. Sci. Technol.* **2018**, *52*, 381−396.

(3) Parry, S.; O'Brien, L.; Fellerman, A.; Eaves, C.; Milestone, N.; Bryan, N.; Livens, F. Plutonium behaviour in nuclear fuel storage pond effluents. *Energy Environ. Sci.* **2011**, *4*, 1457−1464.

(4) Winstanley, E.; Morris, K.; Abrahamsen-Mills, L.; Blackham, R.; Shaw, S. U(VI) sorption during ferrihydrite formation: Underpinning radioactive effluent treatment. *J. Hazard. Mater.* **2019**, *366*, 98−104.

(5) Cornell, R.; Schwertmann, U. *The iron oxides: structure, properties, reactions, occurrences and uses*; Wiley-VCH: Weinheim, Germany, 2004.

(6) Zhao, J.; Huggins, F. E.; Feng, Z.; Huffman, G. P. Ferrihydrite: surface structure and its effects on phase transformation. *Clay. Clay Miner.* **1994**, *42*, 737−746.

(7) Um, W.; Serne, R.; Brown, C.; Rod, K. Uranium(VI) sorption on iron oxides in Hanford Site sediment: Application of a surface complexation model. *Appl. Geochem.* **2008**, *23*, 2649−2657.

(8) Bots, P.; Shaw, S.; Law, G.; Marshall, T.; Mosselmans, J.; Morris, K. Controls on the fate and speciation of Np(V) during iron (oxyhydr)oxide crystallization. *Environ. Sci. Technol.* **2016**, *50*, 3382−3390.

(9) Romanchuk, A.; Gusev, I.; Vlasova, I.; Petrov, V.; Kuzmenkova, N.; Egorova, B.; Zakharova, E.; Volkova, A.; Kalmykov, S. Interaction of plutonium with iron- and chromium-containing precipitates under the conditions of reservoir bed for liquid radioactive waste. *Radiochemistry* **2016**, *58*, 662−667.

(10) Sadeghi, O.; Zakharov, L.; Nyman, M. Aqueous formation and manipulation of the iron-oxo keggin ion. *Science* **2015**, *347*, 1359−1362.

(11) Michel, F. M.; Ehm, L.; Antao, S. M.; Lee, P. L.; Chupas, P. J.; Liu, G.; Strongin, D. R.; Schoonen, M. A. A.; Phillips, B. L.; Parise, J. B. The structure of ferrihydrite, a nanocrystalline material. *Science* **2007**, *316*, 1726−1729.

(12) Weatherill, J. S.; Morris, K.; Bots, P.; Stawski, T.; Janssen, A.; Abrahamsen, L.; Blackham, R.; Shaw, S. Ferrihydrite formation: The role of Fe_{13} keggin clusters. *Environ. Sci. Technol.* **2016**, *50*, 9333−9342.

(13) Wilson, P. *The nuclear fuel cycle: from ores to wastes*; Oxford University Press: 1997.

(14) Sylvester, P.; Milner, T.; Jensen, J. Radioactive liquid waste treatment of Fukushima Daiichi. *J. Chem. Technol. Biotechnol.* **2013**, *88*, 1592−15961.

(15) Powell, B.; Fjeld, R.; Kaplan, D.; Coates, J.; Serkiz, S. Pu(V)O_2^+ adsorption and reduction by synthetic magnetite (Fe_3O_4). *Environ. Sci. Technol.* **2004**, *38*, 6016−6024.

(16) Powell, B.; Fjeld, R.; Kaplan, D.; Coates, J.; Serkiz, S. Pu(V)O_2^+ adsorption and reduction by synthetic hematite and goethite. *Environ. Sci. Technol.* **2005**, *39*, 2107−2114.

(17) Hixon, A.; Powell, B. Observed changes in the mechanism and rates of Pu(V) reduction on hematite as a function of total plutonium concentration. *Environ. Sci. Technol.* **2014**, *48*, 9255−9262.

(18) Kirsch, R.; Fellhauer, D.; Altmaier, M.; Neck, V.; Rossberg, A.; Fanghänel, T.; Charlet, L.; Scheinost, A. Oxidation state and local structure of plutonium reacted with magnetite, mackinawite, and chukanovite. *Environ. Sci. Technol.* **2011**, *45*, 7267−7274.

(19) Hu, Y.; Schwaiger, L.; Booth, C.; Kukkadapu, R.; Cristiano, E.; Kaplan, D.; Nitsche, H. Molecular interactions of plutonium(VI) with synthetic manganese-substituted goethite. *Radiochim. Acta.* **2010**, *98*, 655−663.

(20) Romanchuk, A.; Kalmykov, S.; Aliev, R. Plutonium sorption onto hematite colloids at femto- and nanomolar concentrations. *Radiochim. Acta* **2011**, *99*, 137−114.

(21) Romanchuk, A.; Kalmykov, S.; Egorov, A.; Zubavichus, Y.; Shiryaev, A.; Batuk, O.; Conradson, S.; Pankratov, D.; Presnyakov, I. Formation of crystalline $PuO_{2+x}{\cdot}nH_2O$ nanoparticles upon sorption of Pu(V,VI) onto hematite. *Geochim. Cosmochim. Acta* **2013**, *121*, 29−40.

(22) Begg, J.; Zavarin, M.; Kersting, A. Plutonium desorption from mineral surfaces at environmental concentrations of hydrogen peroxide. *Environ. Sci. Technol.* **2014**, *48*, 6201−6210.

(23) Zhao, P.; Begg, J.; Zavarin, M.; Tumey, S.; Williams, R.; Dai, Z.; Kips, R.; Kersting, A. Plutonium(IV) and (V) sorption to goethite at sub-femtomolar to micromolar concentrations: redox transformations and surface precipitation. *Environ. Sci. Technol.* **2016**, *50*, 6948−6956.

(24) Wang, Z.; Ulrich, K.; Pan, C.; Giammar, D. Measurement and Modeling of U(IV) Adsorption to Metal Oxide Minerals. *Environ. Sci. Technol. Lett.* **2015**, *2*, 227−232.

(25) Stetten, L.; Mangeret, A.; Brest, J.; Seder-Colomina, M.; Le Pape, P.; Ikogou, M.; Zeyen, N.; Thouvenot, A.; Julien, A.; Alcalde, G.; Reyss, J.; Bombled, B.; Rabouille, C.; Olivi, L.; Proux, O.; Cazala, C.; Morin, G. Geochemical control on the reduction of U(VI) to mononuclear U(VI) species in lacustrine sediments. *Geochim. Cosmochim. Acta* **2018**, *222*, 171−186.

DOI: 10.1021/acsearthspacechem.9b00105
ACS Earth Space Chem. 2019, 3, 2437−2442

(26) Latta, D.; Mishra, B.; Cook, R.; Kemner, K.; Boyanov, M. Stable U(IV) complexes form at high-affinity mineral surface sites. *Environ. Sci. Technol.* **2014**, *48*, 1683−1691.
(27) Clark, D.; Siegfried, H.; Javinen, G.; Neu, M. In *'Plutonium' in The chemistry of the actinide and transactinide elements*; Morss, L., Edelstein, N., Fuger, J., Eds.; Springer: 2010; Chapter 7.
(28) Stookey, L. Ferrozine - a new spectrophotometric reagent for iron. *Anal. Chem.* **1970**, *42*, 779−781.
(29) Viollier, E.; Inglet, P.; Hunter, K.; Roychoudhury, A.; Van Cappellen, P. The ferrozine method revisited: Fe(II)/Fe(III) determination in natural waters. *Appl. Geochem.* **2000**, *15*, 785−790.
(30) Ravel, B.; Newville, M. Athena, Artemis, Hephaestus: data analysis for X-ray absorption spectroscopy using IFEFFIT. *J. Synchrotron Radiat.* **2005**, *12*, 537−541.
(31) Rehr, J.; Kas, J.; Prange, M.; Sorini, A.; Takimoto, Y.; Vila, F. *Ab initio* theory and calculations of X-ray spectra. *C. R. Phys.* **2009**, *10*, 548−559.
(32) Parkhurst, D.; Appelo, C. Description of input and examples for PHREEQC version 3: a computer program for speciation, batch reaction, one-dimensional transport, and inverse geochemical calculations. *U.S. Geological Survey Techniques and Methods 6* **2013**, *43*, 1−497.
(33) R Core Team. *R: A language and environment for statistical computing*; R Foundation for Statistical Computing: Vienna, Austria, 2016; URL: https://www.R-project.org/.
(34) Charlton, S.; Parkhurst, D. Modules based on the geochemical model PHREEQC for use in scripting and programming languages. *Comput. Geosci.* **2011**, *37*, 1653−1663.
(35) Conradson, S.; Begg, B.; Clark, D.; Auwer, C.; Ding, M.; Dorhout, P.; Espinosa-Faller, F.; Gordon, P.; Haire, R.; Hess, N.; Hess, R.; Koegh, W.; Morales, L.; Neu, M.; Paviet-Hartmann, P.; Runde, W.; Tait, C.; Veirs, D.; Villella, P. Local and nanoscale structure and speciation in the $PuO_{2+x-y}(OH)_{2y}{\cdot}zH_2O$ system. *J. Am. Chem. Soc.* **2004**, *126*, 13443−13458.
(36) Calvin, S. *XAFS for everyone*; CRC: Boca Raton, FL, 2013.
(37) Wyckoff, R. PuO_2. *Crystal Structures* **1963**, *1*, 239−444.
(38) Neck, V.; Kim, J. Solubility and hydrolysis of tetravalent actinides. *Radiochim. Acta* **2001**, *89*, 1−16.
(39) Choppin, G. Actinide speciation in the environment. *J. Radioanal. Nucl. Chem.* **2007**, *273*, 695−703.
(40) Seco, F.; Hennig, C.; Pablo, J.; Rovira, M.; Rojo, I.; Marti, V.; Giménez, J.; Duro, L.; Grive, M.; Bruno, J. Sorption of Th (IV) onto Iron Corrosion Products: EXAFS Study. *Environ. Sci. Technol.* **2009**, *43*, 2825−2830.
(41) Shannon, R. Revised effective ionic radii and systematic studies of interatomic distances in halides and chalcogenides. *Acta Crystallogr., Sect. A: Cryst. Phys., Diffr., Theor. Gen. Crystallogr.* **1976**, *32*, 751−767.
(42) Dumas, T.; Fellhauer, D.; Schild, D.; Gaona, X.; Altmaier, M.; Scheinost, A. Plutonium retention mechanisms by magnetite under anoxic conditions: entrapment versus sorption. *ACS Earth Space Chem.* **2019**, DOI: 10.1021/acsearthspacechem.9b00147.

DOI: 10.1021/acsearthspacechem.9b00105
ACS Earth Space Chem. 2019, 3, 2437−2442